

# Frequency multiplication with toroidal mode number of kink/fishbone modes on a static HL-2A-like tokamak

Zhihui ZOU<sup>1</sup>, Ping ZHU<sup>2,3\*</sup>, Charlson C. KIM<sup>4</sup>, Wei DENG<sup>5</sup>, Xianqu WANG<sup>6</sup>, Yawei HOU<sup>1\*\*</sup>

<sup>1</sup> CAS Key Laboratory of Geospace Environment and Department of Plasma Physics and Fusion Engineering, University of Science and Technology of China, Hefei, 230026, Peoples's Republic of China

<sup>2</sup> International Joint Research Laboratory of Magnetic Confinement Fusion and Plasma Physics, State Key Laboratory of Advanced Electromagnetic Engineering and Technology, School of Electrical and Electronic Engineering, Huazhong University of Science and Technology, Wuhan, 430074, Peoples's Republic of China

<sup>3</sup> Department of Engineering Physics, University of Wisconsin-Madison, Madison, Wisconsin 53706, USA

<sup>4</sup> SLS2 Consulting, San Diego, California 92107, USA

<sup>5</sup> Southwestern Institute of Physics, PO Box 432, Chengdu 610041, People's Republic of China

<sup>6</sup> Institute of Fusion Science, School of Physical Science and Technology, Southwest Jiaotong University, Chengdu, 610031, Peoples's Republic China

## Abstract

In the presence of energetic particles (EPs), the Long-Lived Mode (LLM) frequency multiplication with  $n = 1, 2, 3$  or higher is often observed on HL-2A, where  $n$  is the toroidal mode number. Hybrid kinetic-MHD model simulations of the energetic particle (EP) driven kink/fishbone modes on a static HL-2A-like tokamak using NIMROD code find that, when the background plasma pressure is relatively high, and the EP pressure and the beam energy are relatively low, the mode frequency increases almost linearly with EP pressure, and the frequency is proportional to  $n$  ("frequency multiplication"), even in absence of any equilibrium plasma rotation. In addition, the frequency multiplication persists as the safety factor at magnetic axis  $q_0$  varies. In absence of EPs, the growth rate of the 1/1 mode

is the largest; however, as the EP pressure increases, the growth rate of 2/2 modes or 3/3 modes becomes dominant, suggesting that the higher- $n$  modes are more vulnerable to EPs. These results may shed light on the understanding about the toroidal mode number dependence of kink/fishbone modes in the advanced scenarios of tokamaks with weak or reversed central magnetic shear.

**Keywords:** internal kink mode, fishbone mode, Long-Lived Mode(LLM), energetic particles(EPs), HL-2A, NIMROD

(Some figures may appear in colour only in the online journal)

## 1 Introduction

Confinement improvement and higher beta limit have been achieved in advanced tokamak (AT) operation scenarios, in which the  $q$ -profile is reversely or weakly sheared in the core region [1–3], and the AT operation scenarios have been proposed for the steady-state operation of ITER [4, 5]. With weak shear and plasma pressure gradient exceeding a critical value in the core region, besides 1/1 internal kink mode [6–8], higher-harmonics modes, which are usually called “infernal modes” [9, 10], also become unstable. Fishbone modes, which are believed to be driven by the resonant interaction between internal kink mode and the energetic particles (EPs) [11–14], have been observed on many tokamaks with auxiliary heating since 1980s [15–19]. During the fishbone burst events, which usually last about 1 millisecond, significant loss of EPs has been observed, and they degrade the heating efficiency and limit the beta achieved in the experiments. Besides, the lost EPs can cause the damage of the first wall. The time interval between two adjacent fishbone bursts is usually several milliseconds, and the  $q$ -profile is monotonic with finite shear in the core region. Similar to the energetic particle (EP) driven fishbone modes, another kind of EP driven modes are observed in auxiliary heating experiments with flat  $q$  in the core plasma. The modes last 100 milliseconds or longer after the saturation, which are called long-lived modes (LLMs) for the long-lasting feature. The LLMs often cause loss of EPs and

braking of the plasma toroidal rotation. Unlike the bursty fishbone modes, the LLMs may serve as an option for the AT operation scenarios because of the gentle and continuous energy loss in the core plasma of tokamaks.

Because the potential for the AT operation scenarios, many experiments have been performed to study LLMs. During the NBI heating of plasmas with flat central safety factor profile, LLMs are observed on HL-2A that can last for several hundred milliseconds, and the mode frequency is approximately proportional to the toroidal mode number  $n$ , a phenomenon we refer to as frequency multiplication (FM), as shown in figure 1 of reference [20], where all 1/1, 2/2, 3/3 and 4/4 modes are displayed in the frequency range of 10 kHz  $\sim$  60 kHz. The LLMs can be suppressed by ECRH or SMBI (supersonic molecular beam injection) which is related to changing of  $q$  profile and pressure gradient [20]. On MAST, the FM for LLMs is also observed during NBI heating, not only for weakly sheared, but also for slightly and reversely sheared  $q$ -profiles, where the critical plasma pressure, above which the mode becomes unstable, increases with  $n$  [21]. For KSTAR plasma with ECRH and NBI, the pressure-driven LLMs lasts up to 40 seconds along with the FM, when  $q$ -profile is above 2 with broad weak shear in the core region [22]. As a characteristic feature of LLMs, the FM has not been well understood.

Several analytical or numerical studies have investigated the properties of LLMs. Solving an analytical dispersion relation developed for LLMs based on the HL-2A equilibrium, Zhang *et al* find the growth rate of the 2/2 mode greater than that of the 1/1 mode, and the frequency is proportional to  $n$  ( $n = 1, 2, 3$ ) [23]. However, they have not considered the FM in detail, and the 3/3 mode is stable in their calculations, different from the experimental observations. Including the equilibrium rotation in the dispersion relation, Xie reports that fishbone mode can turn into LLM with low magnetic shear, when the EP pressure and the plasma rotation frequency both exceed certain critical value [24], however, neither the  $n > 1$  mode or the FM is discussed. Using the kinetic-MHD hybrid code M3D-K

for simulations of a circular cross-section tokamak with central weakly sheared  $q$ -profile, Ren *et al* obtain the FM of LLMs in the presence of EPs, where the growth rates of higher harmonics ( $n > 1$ ) can be greater than 1/1 mode [25]. Their study is based on the analytical equilibrium profile for a model tokamak, and the conditions in which the FM is broken remains unclear.

In this work, we study the FM of LLMs, with a focus on its onset conditions. Based on the equilibrium generated from the LLM experiments on HL-2A, using the hybrid kinetic-MHD model implemented in the NIMROD code [26–28], our simulations show that the EP-driven fishbone mode frequency is almost proportional to  $n$  in absence of any equilibrium toroidal flow, and the FM appears when the background plasma pressure gradient is above certain threshold, but neither the beam energy or the EP  $\beta$  fraction (the ratio between EP pressure and total plasma pressure) is too high. The 1/1 mode is the most unstable when the EP pressure is not too high [29]. However, higher- $n$  kink/fishbone modes are found more dominant when EP pressure becomes relatively high.

The rest of paper is organized as follows. The simulation model is reviewed briefly in section 2. The simulation set-up is described in section 3, which is followed by the report on the main results in section 4. First, the  $q_0$  effect on kink/fishbone mode is studied in both absence or presence of EPs, and then the effects of EP  $\beta$  fraction, beam energy, and EP pressure gradient are also investigated. The summary and discussion are provided in section 5.

## 2 Simulation model

The simulation model is based on the following hybrid kinetic-MHD equations implemented in the NIMROD code [26, 27].

$$\frac{\partial \rho}{\partial t} + \nabla \cdot (\rho \mathbf{V}) = 0 \quad (1)$$

$$\rho \left( \frac{\partial \mathbf{V}}{\partial t} + \mathbf{V} \cdot \nabla \mathbf{V} \right) = \mathbf{J} \times \mathbf{B} - \nabla p_b - \nabla \cdot \mathbf{P}_h \quad (2)$$

$$\frac{n}{\Gamma - 1} \left( \frac{\partial T}{\partial t} + \mathbf{V} \cdot \nabla T \right) = 0 \quad (3)$$

$$\frac{\partial \mathbf{B}}{\partial t} = -\nabla \times \mathbf{E} \quad (4)$$

$$\nabla \times \mathbf{B} = \mu_0 \mathbf{J} \quad (5)$$

$$\mathbf{E} = -\mathbf{V} \times \mathbf{B} \quad (6)$$

where  $\rho$ ,  $\mathbf{V}$ ,  $\mathbf{J}$ ,  $p_b$ ,  $n$  and  $T$  are the mass density, center of mass velocity, current density, plasma pressure, number density, and temperature of the main species plasma,  $\mathbf{E}$  and  $\mathbf{B}$  are the electric and magnetic fields,  $\Gamma$  and  $\mu_0$  are the specific heat ratio and the vacuum permeability, respectively. Static equilibrium is considered in order to exclude effects from the equilibrium rotations. For  $n_h \ll n_b$  and  $\beta_h \sim \beta_b$ , where  $n_b$  ( $n_h$ ) is the main species plasma (energetic particle) number density, and  $\beta_b$  ( $\beta_h$ ) is the ratio of main species background plasma (energetic particle) pressure to magnetic pressure, the pressure tensor  $\mathbf{P}_h$  in the momentum equation can couple the kinetic effects from EPs, which are governed by the drift-kinetic equation [27]. Here  $\mathbf{P}_h = \mathbf{P}_{h0} + \delta \mathbf{P}_h$ , where  $\mathbf{P}_{h0}$  is assumed isotropic, and  $\delta \mathbf{P}_h$  is defined as

$$\delta \mathbf{P}_h = \begin{pmatrix} \delta p_{\perp} & 0 & 0 \\ 0 & \delta p_{\perp} & 0 \\ 0 & 0 & \delta p_{\parallel} \end{pmatrix} \quad (7)$$

$\delta p_{\perp}$  is pressure due to hot particle motions perpendicular to the magnetic field, and  $\delta p_{\parallel}$  is pressure due to the hot particle motions parallel to the magnetic field.

### 3 Simulation setup

An EFIT equilibrium reconstruction based on HL-2A discharge #16074, is used in our simulation [20]. The equilibrium flux surfaces and the mesh in magnetic flux coordinates within the last closed flux surface (LCFS) are shown in figure 1. Although the LCFS is up-down asymmetric, the flux surfaces are close to circles in the core region. The internal kink/fishbone mode locates in the region  $0 < \sqrt{\psi/\psi_0} < 0.2$ , where the safety factor  $q$ -profile is close to unity along with weak magnetic shear [figure 2(a)]. Here  $\psi$  is the poloidal magnetic flux and  $\psi_0$  is the total poloidal magnetic flux within the LCFS.

[Figure 1 about here.]

[Figure 2 about here.]

The EPs from NBI are initialized with the slowing-down distribution function [27],

$$f_0 = \frac{P_0 \exp\left(\frac{P_\zeta}{\psi_n}\right)}{\varepsilon^{3/2} + \varepsilon_c^{3/2}} \quad (8)$$

where  $P_0$  is the normalization constant,  $P_\zeta = g\rho_{||} - \psi_p$  is the canonical toroidal momentum,  $g = RB_\phi$ ,  $\rho_{||} = mv_{||}/qB$ ,  $\psi_p$  is the poloidal flux,  $\psi_n = h\psi_0$ ,  $\psi_0$  is the total flux and the parameter  $h$  is used to match the spatial profile of the equilibrium,  $\varepsilon$  is the particle energy, and  $\varepsilon_c$  is the critical slowing down energy [30]

$$\varepsilon_c = \left(\frac{3}{4}\right)^{2/3} \left(\frac{\pi m_i}{m_e}\right)^{1/3} T_e \quad (9)$$

with  $m_i$  being the ion mass,  $m_e$  the electron mass, and  $T_e$  the electron temperature. Beam ions collide dominantly with the background electrons (ions) for  $\varepsilon > \varepsilon_c$  ( $\varepsilon < \varepsilon_c$ ).

The EPs are loaded into the physical space following the profile  $p = p_0 \exp(-h\psi/\psi_0)$ , where  $p_0$  is pressure at magnetic axis, EP pressure gradient becomes higher as  $h$  decreases [figure 2(b)]. For linear simulations, we set resistivity  $\eta = 0$ , and a total  $10^6$  simulation particles are prescribed in the poloidal

plane with  $64 \times 64$  finite elements. Other main parameters are input from equilibrium [23], with the major radius  $R = 1.65$  m, the minor radius  $a = 0.40$  m, the toroidal magnetic field  $B_0 = 1.37$  T, and the number density is set to be constant in the radial direction with  $n = 2.44 \times 10^{19} \text{ m}^{-3}$ . The case with  $q_0 = 0.9$ ,  $\beta_f = \beta_h/\beta_0 = 0.1$ ,  $h = 0.25$  and beam energy  $\varepsilon_b = 10\text{keV}$  is specified as the standard reference case for comparisons.

## 4 Simulation results

LLMs are observed on the experiments with NBI heating, and they can be controlled by ECRH and SMBI, subject to the influences from magnetic shear, pressure gradient and NBI beam properties [20]. In order to investigate these effects in our simulations, we scan  $q_0$  to study effects of magnetic shear on FM for LLMs, and the EP beta fraction  $\beta_f$ , beam energy  $\varepsilon_b$  and EP pressure gradient to study the effects of EPs on FM. We choose two representative time moments of the discharge #016074, one is at 420 ms (M420), and the another is at 452 ms (M452). The M420 case is at early stage of the mode growth, and the M452 case is near the saturation of the mode, as shown in the figure 1 of reference [20]. The pressure gradient profiles of the M420 and M452 cases are shown in figure 3. The pressure gradient of the M420 case is almost two times of that of the M452 case. We use the two pressure profiles to study the effects of background plasma pressure gradient on FM.

[Figure 3 about here.]

### 4.1 $q_0$ effects in absence of EPs

First we scan  $q_0$  to study its effects on the modes without EP. As shown in figure 4, varying  $q_0$  along shifts the  $q$ -profile up or down entirely with minimal change in its shape.

[Figure 4 about here.]

For the two equilibria from the M420 and M452 case, linear NIMROD calculations show that the  $m/n = 1/1, 2/2$  and  $3/3$  kink modes are unstable when  $q_0 < 1$  in absence of energetic particles, where  $m$  is the poloidal mode number. The linear growth rate of kink modes decreases with  $n$ , namely,  $\gamma_{1/1} > \gamma_{2/2} > \gamma_{3/3}$ . As  $q_0$  increases, the growth rate increases first and then decreases to zero as  $q_0$  approaches unity. The  $q_{0max}$ , the value of  $q_0$  at which the growth rate reaches the maximum, increases with  $n$  (figure 5). The contour plots of the plasma pressure perturbation for the M452 case (figure 6) show that the mode structure shrinks in size as  $q_0$  approaches to unity. The contour plots for the M420 case are similar, and thus are not repeated here. For the  $1/1$  kink mode, the mode structure is global within the  $q < 1$  region. For  $2/2$  and  $3/3$  kink modes, the mode structures become more localized around  $q = 1$  surface, which is consistent with the theory prediction [31].

In absence of EPs, these MHD modes are purely growing instabilities without real frequency or FM phenomenon. This is in agreement with the observation that LLMs only occur in presence of NBI heating or other auxiliary heating.

[Figure 5 about here.]

[Figure 6 about here.]

## 4.2 $q_0$ effects in presence of EPs

Now we study the  $q_0$  effects on the modes in presence of EPs, and set  $\beta_f = 0.1$ . For the M420 case in presence of EPs, the overall growth rates become higher [figure 7(a)]. The mode frequency increases slightly as  $q_0$  increases, and more importantly, the FM exists for  $n = 1, n = 2$  and  $n = 3$  [figure 7(b)], which is consistent with the experiment observation in HL-2A [23]. For the M452 case, as shown in figure 7(c), the  $1/1$  and  $2/2$  kink modes are more stable in presence of EPs, whereas only the  $3/3$  mode is driven more unstable by EPs. The FM remains with  $n = 1$  and  $n = 2$ . However for the  $3/3$  mode, the mode frequency difference from the  $2/2$  mode is significantly larger than the frequency



interval between 2/2 and 1/1 modes [figure 7(d)]. Comparing the results of M420 and M452, we find that stronger background plasma pressure gradient maintains the FM for  $n = 1, 2, 3$  (as in the M420 case), which becomes weakened with weaker background plasma pressure gradient (as in the M452 case). This is consistent with experimental findings that LLMs are characteristic of pressure-driven modes [20]. Comparing the results from section 4.1, we have found FM in presence of EPs, and FM is weakened or broken with reduced background plasma pressure gradient.

[Figure 7 about here.]

Comparing figure 7 in this paper and figure 1 in reference [20] carefully, we find that the frequency range does not match, although FM exists in both figures. The main reason is that we have not considered plasma rotation. According to  $f_{\text{exp}} = f_{\text{EP}} + n f_{\text{rot}}$ , where  $f_{\text{exp}}$  is the frequency measured in the experiments,  $f_{\text{EP}}$  is the frequency caused by EPs, and  $f_{\text{rot}}$  is the frequency of plasma rotation. Adding the frequencies from the simulations ( $f_{1/1}^{\text{sim}} \simeq 2.5$  kHz,  $f_{2/2}^{\text{sim}} \simeq 6$  kHz and  $f_{3/3}^{\text{sim}} \simeq 9$  kHz) and frequency of plasma rotation ( $f_{\text{rot}} \simeq 7$  kHz as measured in the experiments [20]), we get  $f_{1/1} \simeq 10$  kHz,  $f_{2/2} \simeq 20$  kHz and  $f_{3/3} \simeq 30$  kHz, which are close to the frequencies measured in the experiments.

For the M420 case, the mode structures shown in figure 8 are similar to the cases in absence of EPs as shown in figure 6, except that they are now twisted by EPs, which become more significant as  $n$  increases and  $q_0$  approaches to unity. For the M452 case, the poloidal mode structures twisting by EPs are more apparent in comparison to the M420 case. For the  $n = 3$  mode, the structure of mode coupling appears [figure 9 (a3), (b3) and (c3)], which is indicative of the toroidal Alfvén eigenmode (TAE).

[Figure 8 about here.]

[Figure 9 about here.]

### 4.3 Effects of EP $\beta$ fraction $\beta_f$

We set  $q_0 = 0.9$ , and scan  $\beta_f$  to study EP pressure effects on the modes. For the M420 case, as the EP  $\beta_f$  increases, the growth rate of higher- $n$  mode increases more rapidly. As the EP pressure increases, the growth rates of higher- $n$  mode approach to that of 1/1 mode, and for  $\beta_f > 0.25$ , the growth rate of 3/3 mode becomes the largest [figure 10(a)]. This indicates that higher- $n$  modes are more vulnerable to EP  $\beta$  effects. When the EP pressure is relatively low ( $\beta_f < 0.2$ ), the mode frequency increases almost linearly with  $\beta_f$ , and is roughly proportional to  $n$ . As  $\beta_f$  increases to 0.25, the frequency of 3/3 mode jumps from  $\sim 10\text{kHz}$  to  $\sim 70\text{kHz}$ , and then decreases as  $\beta_f$  increases further [figure 10 (b)].

[Figure 10 about here.]

For the M452 case, the 1/1 modes and 2/2 modes are suppressed slightly by EPs when the EP pressure is relatively low ( $\beta_f < 0.1$ ); however, there is no suppressing effect on the 3/3 mode. As the EP pressure increases further ( $\beta_f > 0.2$ ), the growth rate of 3/3 mode becomes largest [figure 10(c)], which is similar to the M420 case. For the 1/1 and 2/2 modes, the mode frequency increases almost linearly with  $\beta_f$ , and is roughly proportional to  $n$ , which is also similar to the M420 case. The frequency of the 3/3 mode jumps to a higher branch ( $\sim 60\text{ kHz}$ ) when  $\beta_f$  increases from 0 to 0.1, and the frequency jumping occurs with  $\beta_f$  smaller than that of the M420 case [figure 10(d)]. For the M420 case, mode structure is twisted by EPs when  $\beta_f < 0.2$ , and there exists poloidal mode coupling for the  $n = 3$  blue mode when  $\beta_f = 0.3$  [figure 11 (a1), (b1) and (c1)]. For the M452 case, the mode structure is twisted by EPs, and there exists poloidal mode coupling for the  $n = 3$  mode when  $\beta_f \geq 0.1$  [figure 11 (a2), (b2) and (c2)].

[Figure 11 about here.]

Comparing the results of the M420 and M452 cases, we can see that, with stronger background plasma pressure gradient (M420), the suppressing effects of EPs on kink modes disappear, and the

driving effects of EPs on higher frequency modes become weaker. Further more, the FM persists for  $n = 1, 2, 3$  up to  $\beta_f < 0.2$  for the stronger background plasma pressure gradient (M420 case), while it is broken for  $n = 3$  with  $\beta_f > 0.1$  for the weaker background plasma pressure gradient (M452 case). This is consistent with results in Section 4.2 that the FM of LLMs becomes more apparent with stronger pressure gradient.

#### 4.4 Effects of beam energy $\varepsilon_b$

Now we scan beam energy  $\varepsilon_b$  to study its effects on FM, and we set  $q_0 = 0.9$  and  $\beta_f = 0.1$ . For the M420 case, the growth rate decreases with the beam energy  $\varepsilon_b$  when the mode frequency is low ( $\sim 10$  kHz) [figure 12(a)]. When beam energy  $\varepsilon_b$  is less than 15 keV, the mode frequency is proportional to  $n$  approximately. However, for the 3/3 mode, as the beam energy  $\varepsilon_b$  increases from 15 keV to 20 keV, the frequency jumps from 10 kHz to 86 kHz, and the growth rate increases as well suggesting the onset of another branch of mode. For the M452 case, the dependence of growth rate decreases on the beam energy is similar [figure 12(c)]. The FM is broken with  $5 \text{ keV} < \varepsilon_b < 10 \text{ keV}$  for  $n = 3$ , and  $15 \text{ keV} < \varepsilon_b < 20 \text{ keV}$  for  $n = 2$ . Both 2/2 and 3/3 mode frequencies jump to a higher mode branch above certain but different beam energy level.

[Figure 12 about here.]

Comparing the results of the M420 and M452 cases, we can see that, FM can be more easily lost with weaker background plasma pressure gradient [figure 12(b) and figure 12(d)], which is consistent with the results of section 4.2 and 4.3.

#### 4.5 Effects of EP pressure gradient

In the end, we study the effects of EP pressure gradient on FM. For the M420 case, as the EP pressure gradient coefficient  $h$  increases, the radial profile of EPs becomes more flat with smaller EP pressure

gradient and the growth rate decreases [figure 13(a)]. The mode frequency decreases slightly with  $h$ , and remains to be proportional to  $n$  clearly [figure 13(b)]. For the M452 case, the effects of  $h$  on the growth rate are similar, but is much weaker on the mode frequency. The mode frequency keeps almost constant as  $h$  increases. For  $n = 1, 2$ , the mode frequencies are low ( $\sim 10$  kHz), and proportional to  $n$  approximately. For  $n = 3$ , the mode frequency ( $\sim 60$  kHz) can stay on the higher branch for a wide range of EP pressure gradient [figure 13(d)]. Based on the above results, the pressure gradient driven nature of FM for LLMs has been further confirmed and the FM is not much influenced by the EP pressure gradient, which is probably due to the fact that EP pressure is relatively small comparing to background plasma pressure.

[Figure 13 about here.]

## 5 Conclusion

The ( $n = 1, 2, 3$ ) kink/fishbone mode driven by EPs on HL-2A tokamak is investigated through kinetic-MHD simulations. The mode frequency is found to be proportional to toroidal mode number  $n$  (frequency multiplication, FM) even in the absence of equilibrium flow, when the background plasma pressure gradient is strong, and neither the beam energy or the EP  $\beta$  fraction is too high. Above certain threshold for the EP beam energy or the EP  $\beta$  fraction, the FM becomes broken, and the higher- $n$  modes can transform to the AE branch, and such a transition tends to be facilitated by weaker background plasma pressure. The  $q$  profile with varied  $q_0$  ( $0.85 < q_0 < 0.95$ ) have weak influence on the FM. Although in the absence of EPs, the growth rate of the 1/1 mode is greater than that of the higher- $n$  mode, the growth rate of higher- $n$  mode increases more rapidly with  $\beta_f$  than that of 1/1 mode, suggesting the dominance of higher- $n$  modes in experiments with higher EP fraction.

The frequency range we calculate does not match that from experiments for the lacking of plasma rotation in our simulation model. After adding the frequency of plasma rotation, we get frequen-

cies close to experimental measurements. Although we perform the simulations in the circular cross-section tokamak, our results may also apply to the non-circular cross-section tokamaks, such as DIII-D and EAST, because the LLMs are localized in the core region, where magnetic flux surface is near circular for non-circular cross-section tokamaks. In addition, this work is based on the linear simulations with simplified EP model. In future, we plan on performing nonlinear simulations in order to reveal more physical details of LLMs (such the long-lasting feature) in the advanced tokamaks with weak or reversed central magnetic shear.

## Acknowledgments

We thank Prof. Lu Wang and Dr. Da Li for their helpful discussions and suggestions. We appreciate the assistance from Dr. Haolong Li. We are grateful for the support from the NIMROD team. This work was supported by the National Magnetic Confinement Fusion Program of China (No. 2019YFE03050004), National Natural Science Foundation of China (Nos. 11875253, 11775221, 51821005, 11875018), the Fundamental Research Funds for the Central Universities (Nos. WK3420000004 and 2019kfyXJJS193), the Collaborative Innovation Program of Hefei Science Center, CAS (No. 2019HSC-CIP015), the U.S. Department of Energy (Nos. DE-FG02-86ER53218 and DE-SC0018001). This research used the computing resources from the Supercomputing Center of University of Science and Technology of China.

## References

- [1] Taylor T S 1997 *Plasma Phys. Control. Fusion* **39** B47
- [2] Gormezano C *et al* 2004 *Plasma Phys. Control. Fusion* **46** B435

- [3] Sips A C C, for the Steady State Operation and the Transport Physics topical Groups of the ITPA  
2005 *Plasma Phys. Control. Fusion* **47** A19
- [4] Gormezano C *et al* 2007 *Nucl. Fusion* **47** S285
- [5] Kikuchi M 2012 *Rev. Mod. Phys.* **84** 1807
- [6] Shafranov V D 1970 *Sov. Phys. Tech. Phys.* **15** 175
- [7] Rosenbluth M N 1973 *Phys. Fluids* **16** 1894
- [8] Bussac M N *et al* 1975 *Phys. Rev. Lett.* **35** 1638
- [9] Holties H A *et al* 1996 *Nucl. Fusion* **36** 973
- [10] Manickam J *et al* 1987 *Nucl. Fusion* **27** 1461
- [11] Chen L, White R B and Rosenbluth M N 1984 *Phys. Rev. Lett.* **52** 1122
- [12] Coppi B and Porcelli F 1986 *Phys. Rev. Lett.* **57** 2272
- [13] Betti R and Freidberg J P 1993 *Phys. Rev. Lett.* **70** 3428
- [14] Wang S J 2001 *Phys. Rev. Lett.* **86** 5286
- [15] McGuire K *et al* 1983 *Phys. Rev. Lett.* **50** 891
- [16] Heidbrink W W and Sager G 1990 *Nucl. Fusion* **30** 1015
- [17] Nave M *et al* 1991 *Nucl. Fusion* **31** 697
- [18] Chen W *et al* 2010 *Nucl. Fusion* **50** 084008
- [19] Xu L Q *et al* 2015 *Phys. Plasmas* **22** 122510
- [20] Deng W *et al* 2014 *Nucl. Fusion* **54** 013010

- [21] Chapman I T *et al* 2010 *Nucl. Fusion* **50** 045007
- [22] Lee S G *et al* 2016 *Phys. Plasmas* **23** 052511
- [23] Zhang R B *et al* 2014 *Plasma Phys. Control. Fusion* **56** 095007
- [24] Xie W C 2022 *Phys. Rev. E* **105** 055208
- [25] Ren Z Z *et al* 2017 *Phys. Plasmas* **24** 052501
- [26] Sovinec C R *et al* 2004 *J. Comput. Phys.* **195** 355
- [27] Kim C C and the NIMROD team 2008 *Phys. Plasmas* **15** 072507
- [28] Brenna D P, Kim C C and La Haye R J 2012 *Nucl. Fusion* **52** 033004
- [29] Zou Z H *et al* 2021 *Plasma Sci. Technol.* **23** 095107
- [30] Goldston R J and Rutherford P H 2020 *Introduction to Plasma Phys.* (Boca Roton: CRC Press)
- [31] Rosenbluth M N and Rutherford P H 1975 *Phys. Rev. Lett.* **34** 1428

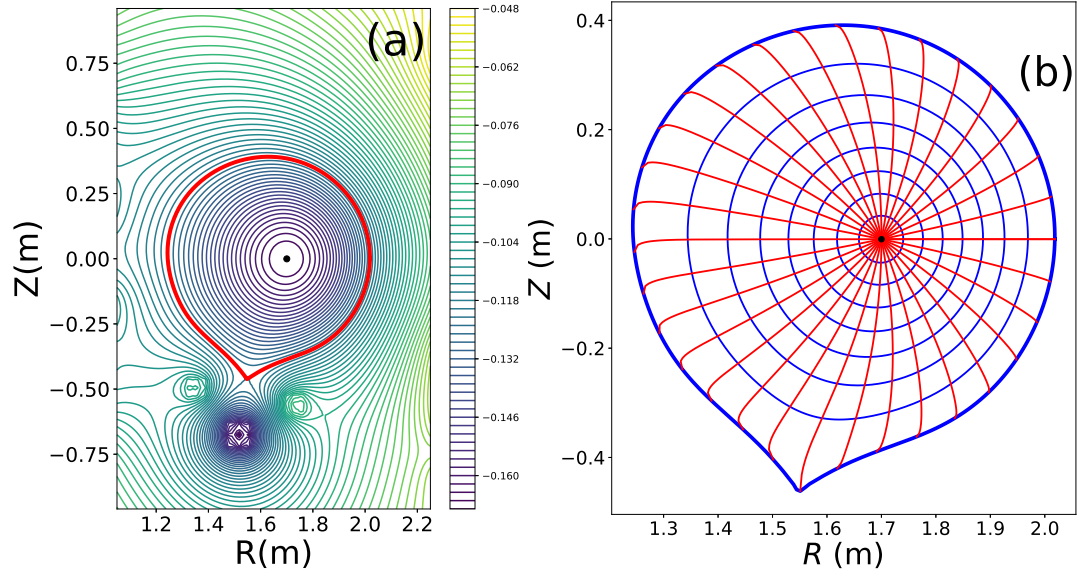


Figure 1: (a) Contour plot of equilibrium poloidal flux with LCFS (the red curve). (b) The sketch map of flux coordinates with uniform poloidal flux and equal poloidal arc length.



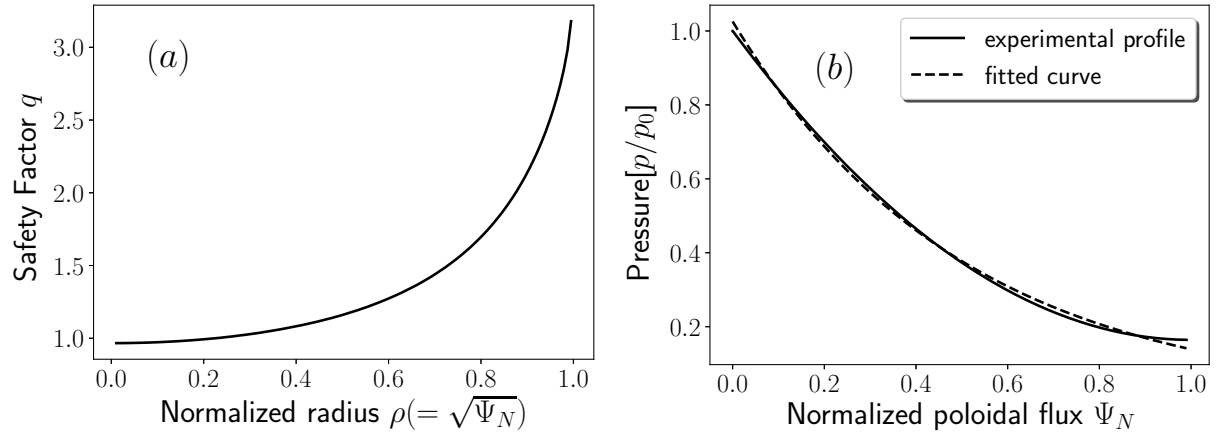


Figure 2: (a) The safety factor profile and (b) pressure profile in HL-2A discharge #16074 at moment 452 (M452).

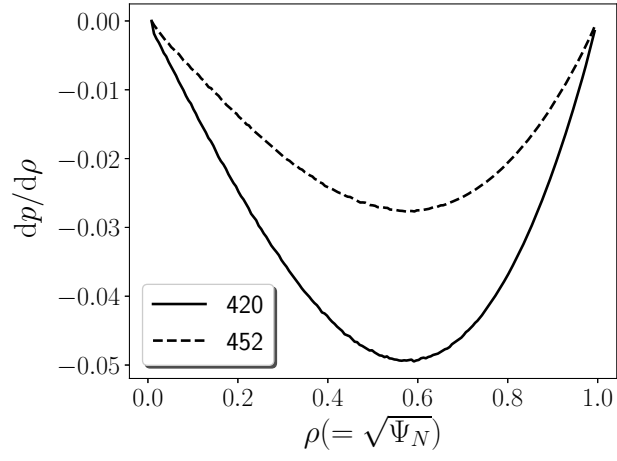


Figure 3: The pressure gradient profiles of equilibriums M420 and M452 from discharge #016074, respectively.

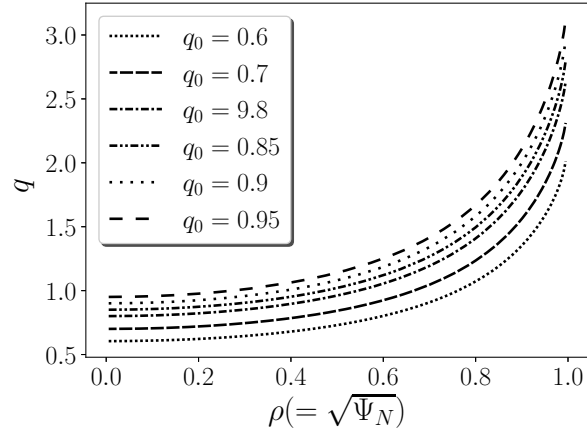


Figure 4:  $q$ -profiles with different  $q_0$ .

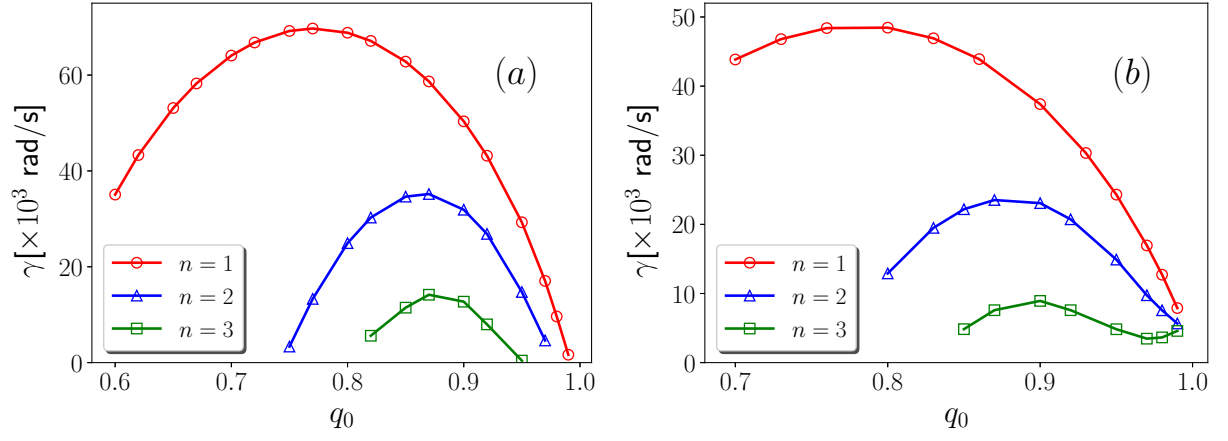


Figure 5: The growth rate as a function of  $q_0$  for  $m/n = 1/1, 2/2, 3/3$  modes in (a) the M420 and (b) the M452 equilibria, respectively.

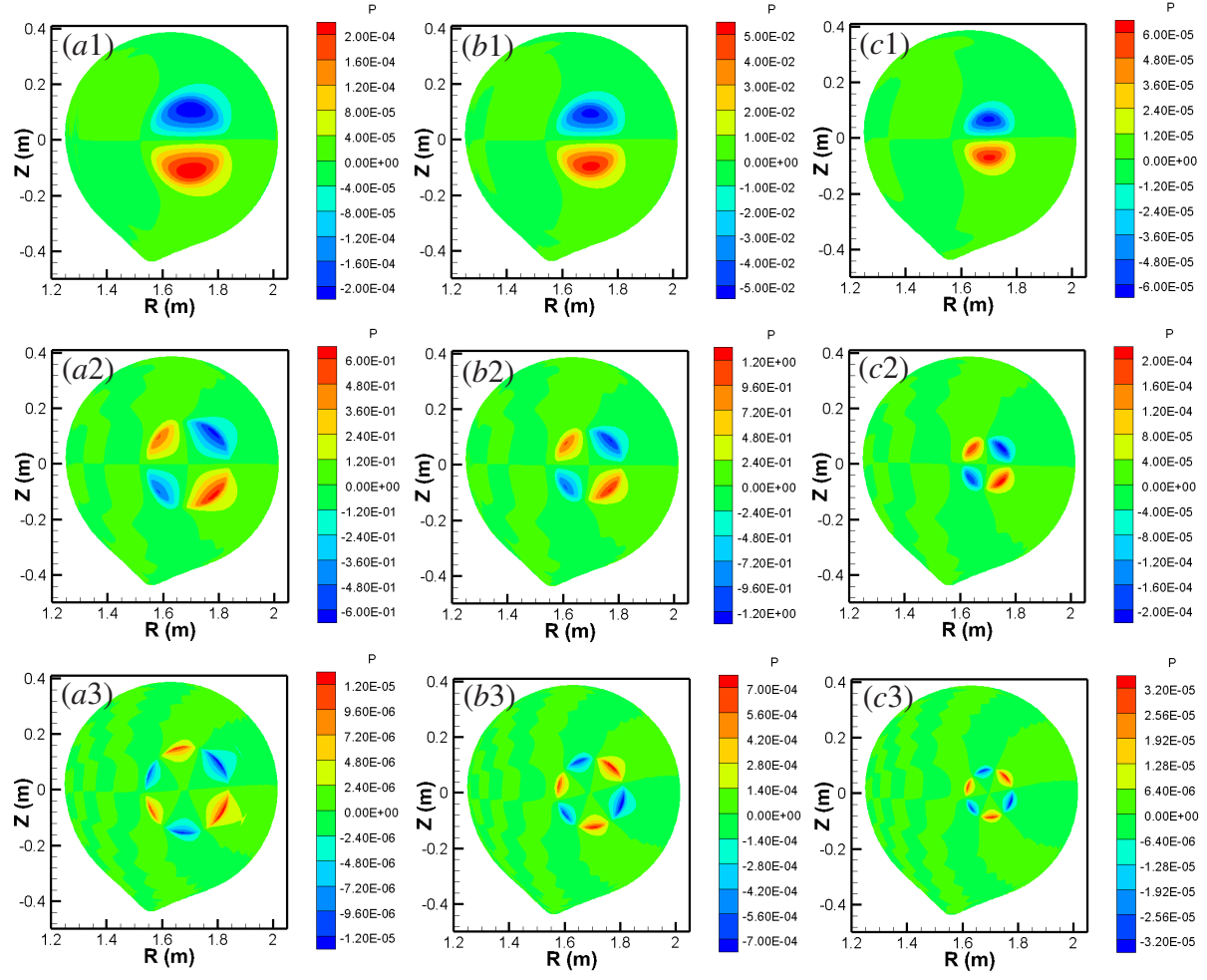


Figure 6: Pressure perturbation contours of the 1/1 modes [(a1), (b1) and (c1)], the 2/2 modes [(a2), (b2) and (c2)] and the 3/3 modes [(a3), (b3) and (c3)] with  $q_0 = 0.85$  [(a1), (a2) and (a3)],  $q_0 = 0.9$  [(b1), (b2) and (b3)] and  $q_0 = 0.95$  [(c1), (c2) and (c3)] based on the M452 equilibrium.

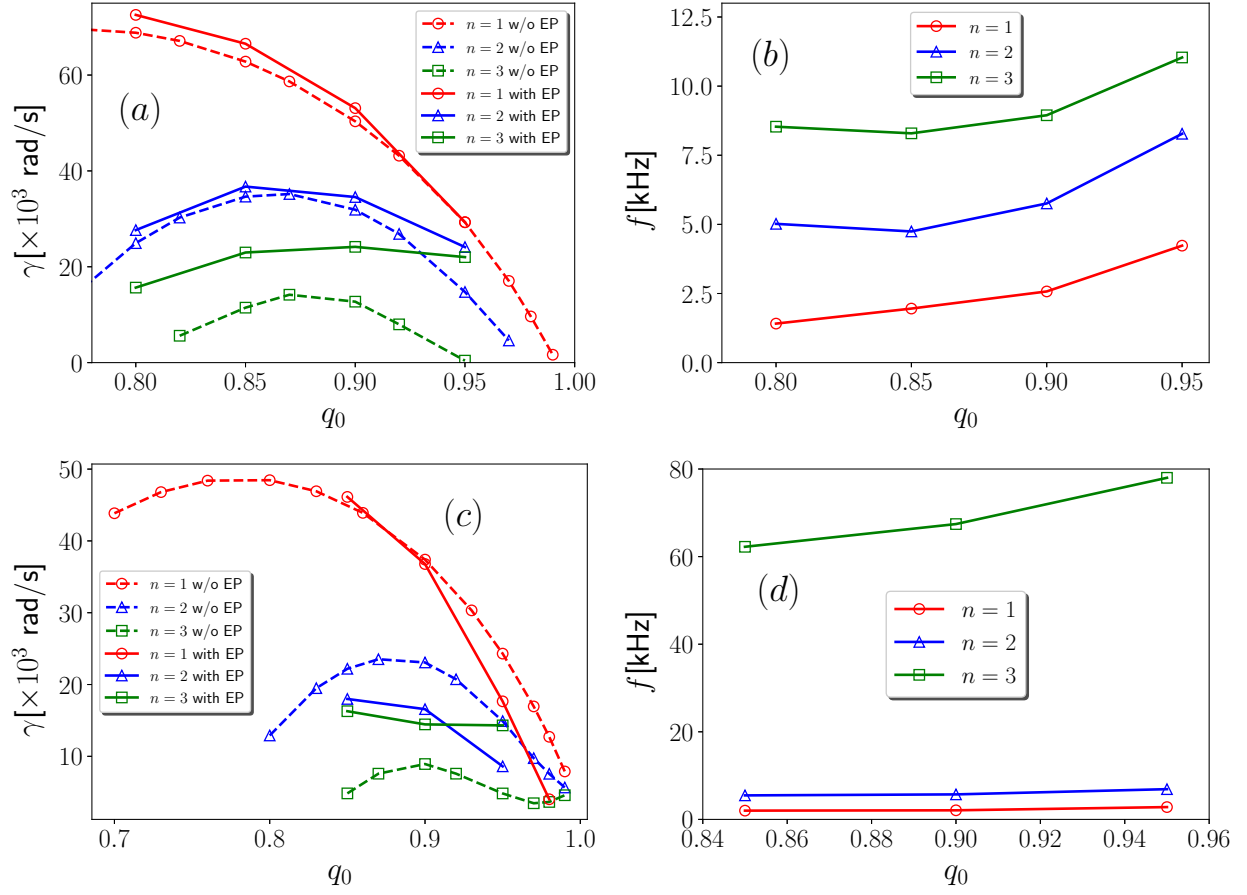


Figure 7: Growth rates [(a) and (c)] and mode frequencies [(b) and (d)] as functions of  $q_0$  for the 1/1, 2/2 and 3/3 modes, where  $\beta_f = 0.1$ . (a) and (b) are based on the M420 equilibrium, (c) and (d) are based on the M452 equilibrium.

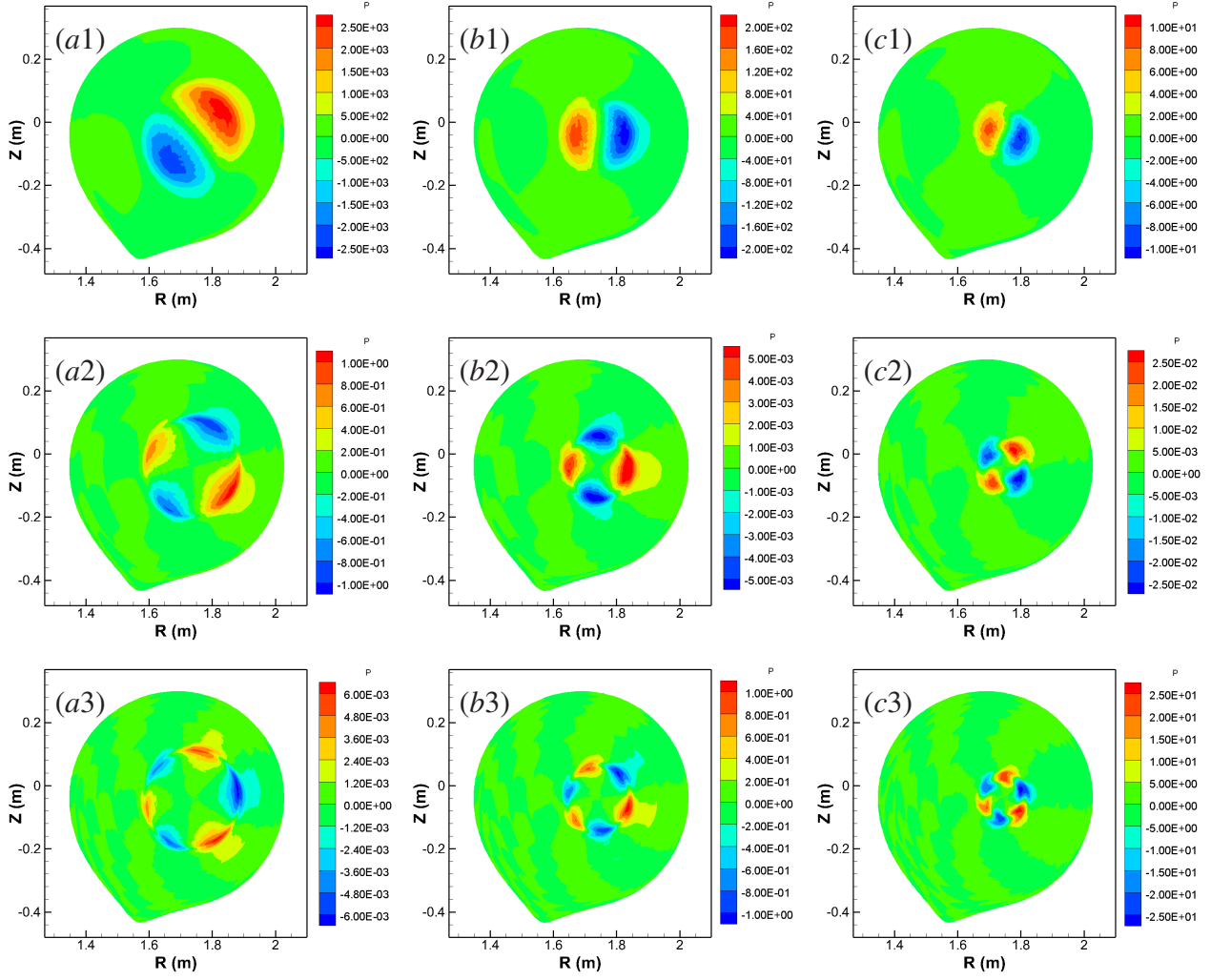


Figure 8: Pressure perturbation contours of the 1/1 modes [(a1), (b1) and (c1)], the 2/2 modes [(a2), (b2) and (c2)] and the 3/3 modes [(a3), (b3) and (c3)] with  $q_0 = 0.8$  [(a1), (a2) and (a3)],  $q_0 = 0.9$  [(b1), (b2) and (b3)] and  $q_0 = 0.95$  [(c1), (c2) and (c3)], where  $\beta_f = 0.1$  based on the M420 equilibrium.

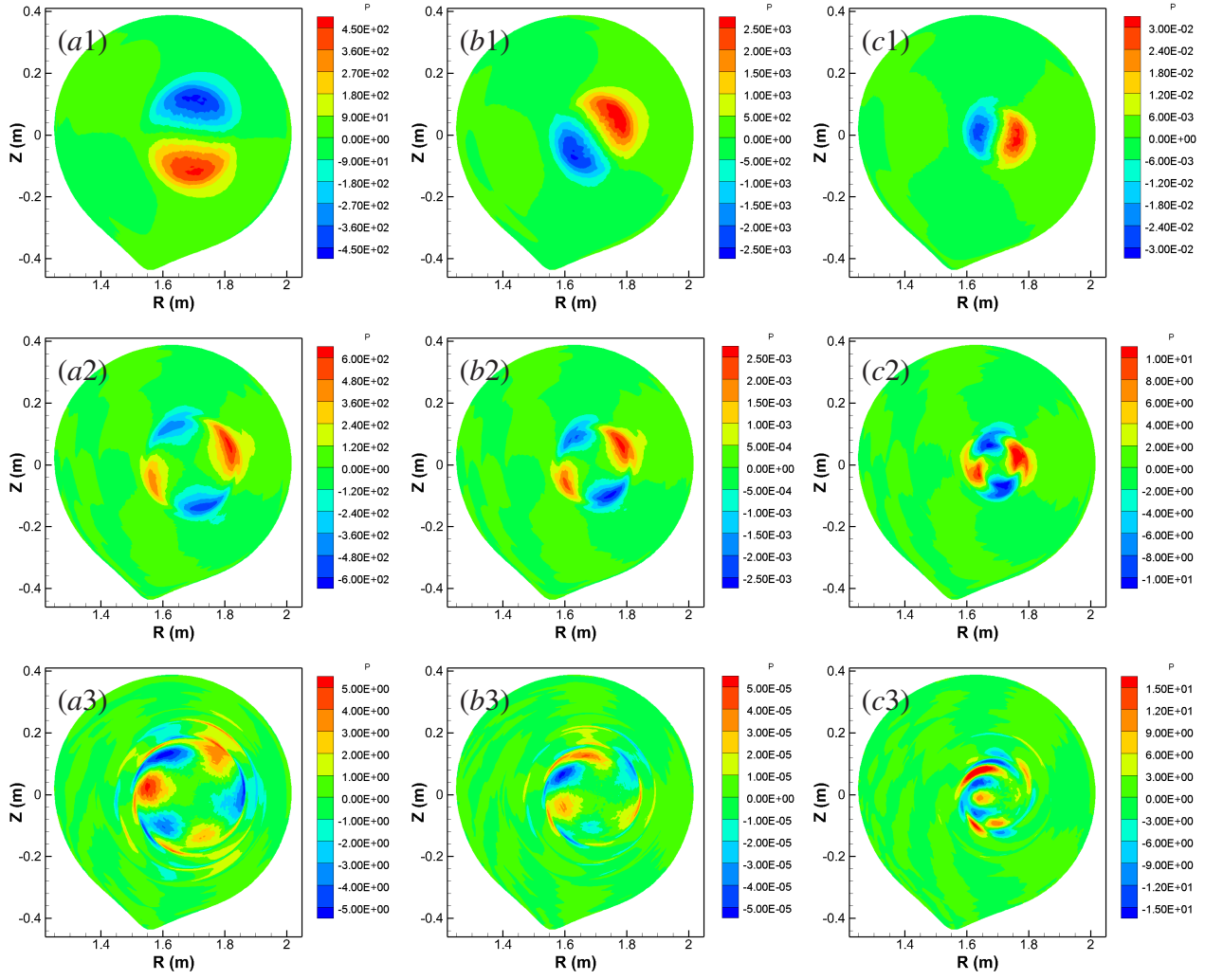


Figure 9: Pressure perturbation contours of the 1/1 modes [(a1), (b1) and (c1)], the 2/2 modes [(a2), (b2) and (c2)] and the 3/3 modes [(a3), (b3) and (c3)] with  $q_0 = 0.85$  [(a1), (a2) and (a3)],  $q_0 = 0.9$  [(b1), (b2) and (b3)] and  $q_0 = 0.95$  [(c1), (c2) and (c3)], where  $\beta_f = 0.1$  based on the M452 equilibrium.



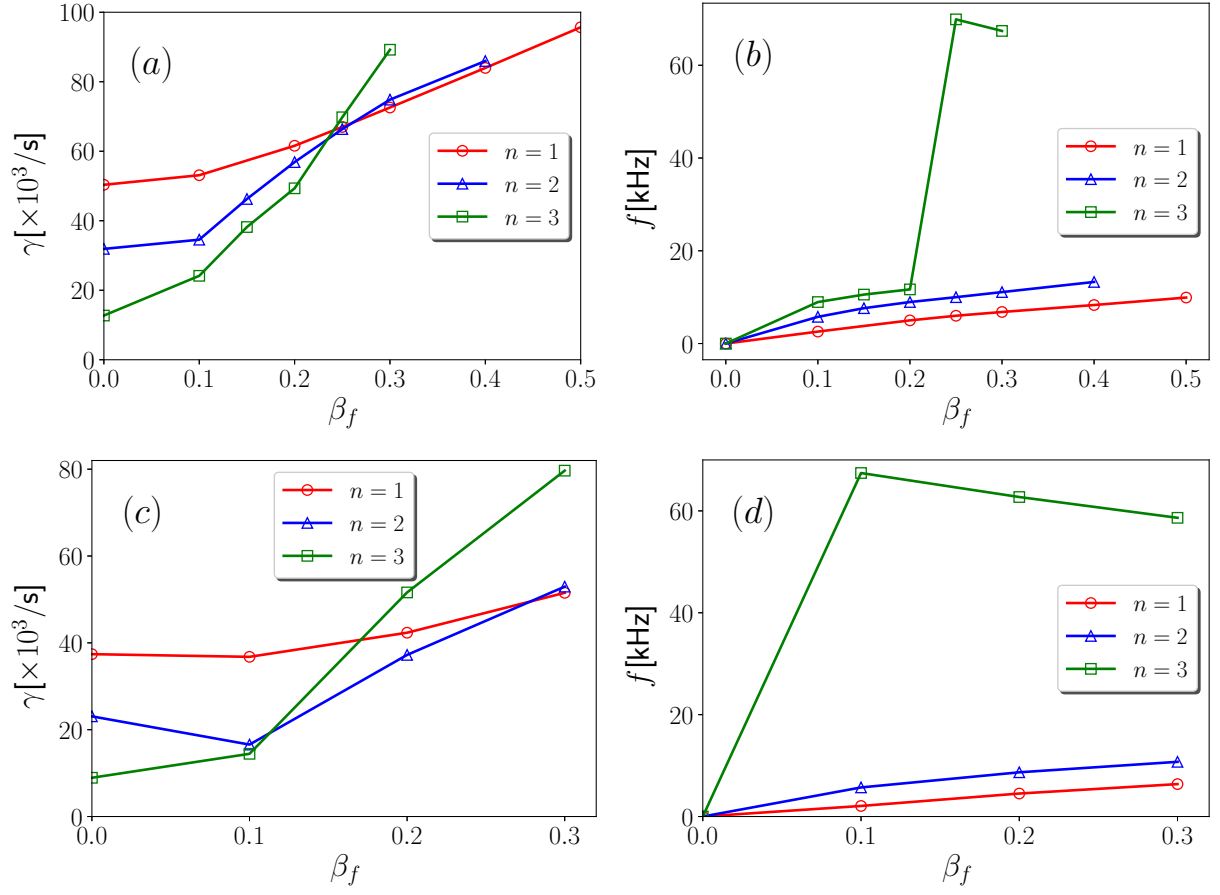


Figure 10: Growth rates [(a) and (c)] and mode frequencies [(b) and (d)] as functions of  $\beta_f$  for the 1/1, 2/2 and 3/3 modes, where  $q_0 = 0.9$ . (a) and (b) are based on the M420 equilibrium, (c) and (d) are based on the M452 equilibrium.

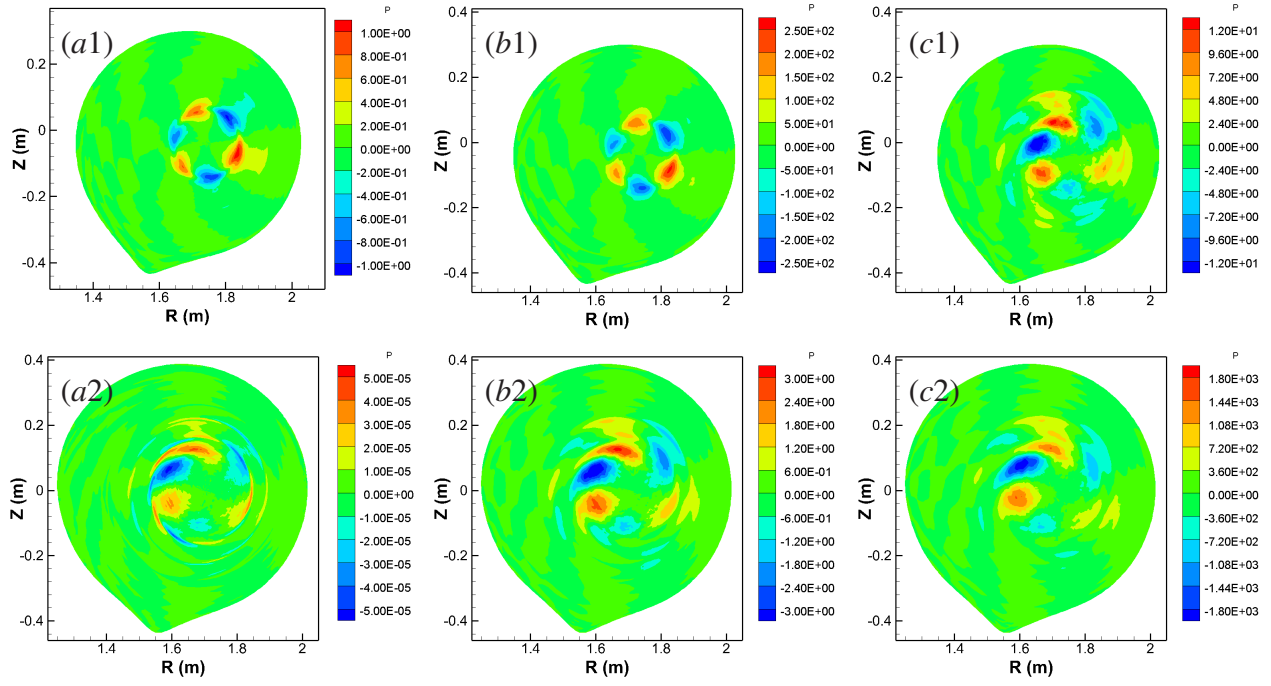


Figure 11: Pressure perturbation contours of the 3/3 modes based on the M420 equilibrium [(a1), (b1) and (c1)], and the M452 equilibrium [(a2), (b2) and (c2)], where  $\beta_f = 0.1$  [(a1) and (a2)],  $\beta_f = 0.2$  [(b1) and (b2)], and  $\beta_f = 0.3$  [(c1) and (c2)].

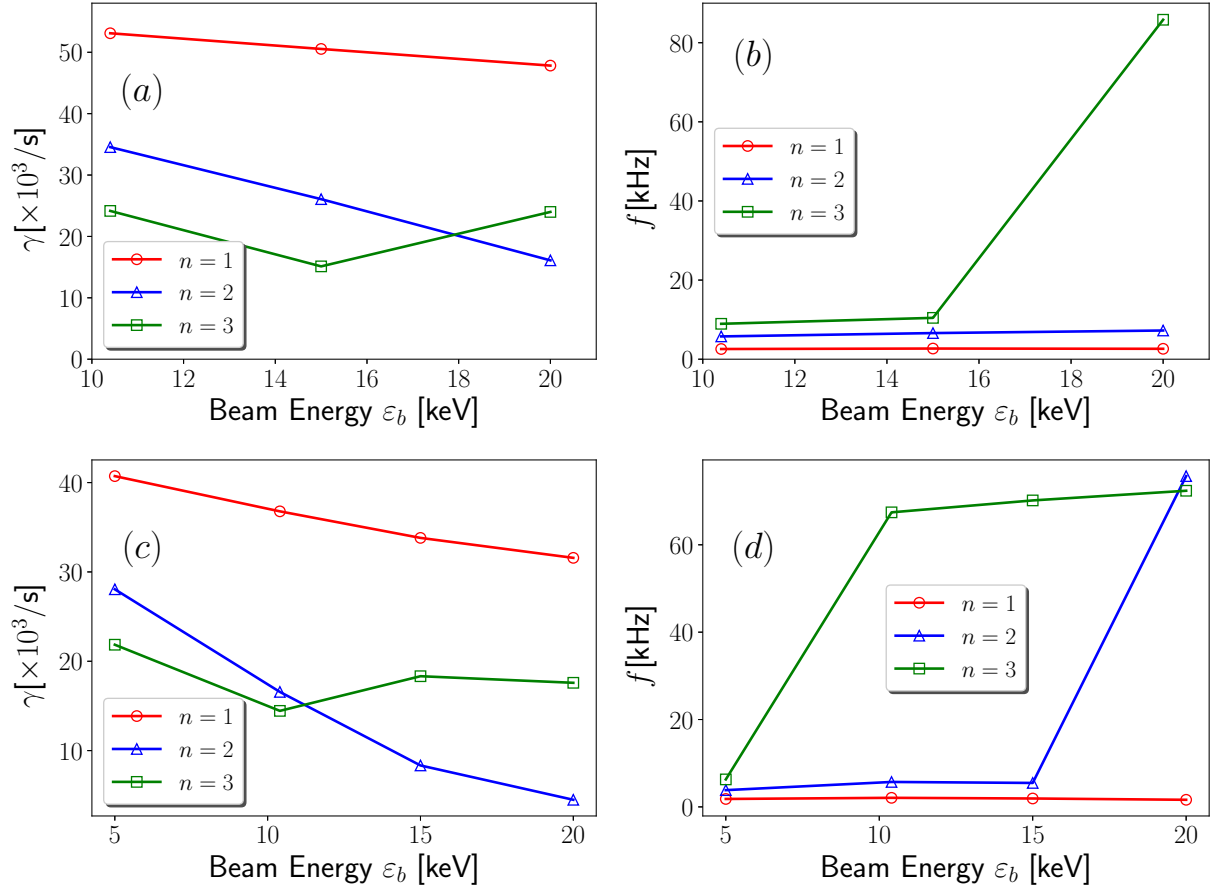


Figure 12: Growth rates [(a) and (c)] and mode frequencies [(b) and (d)] as functions of beam energy  $\varepsilon_b$  for the 1/1, 2/2 and 3/3 modes, where  $q_0 = 0.9$  and  $\beta_f = 0.1$ . (a) and (b) are based on the M420 equilibrium, (c) and (d) are based on the M452 equilibrium.

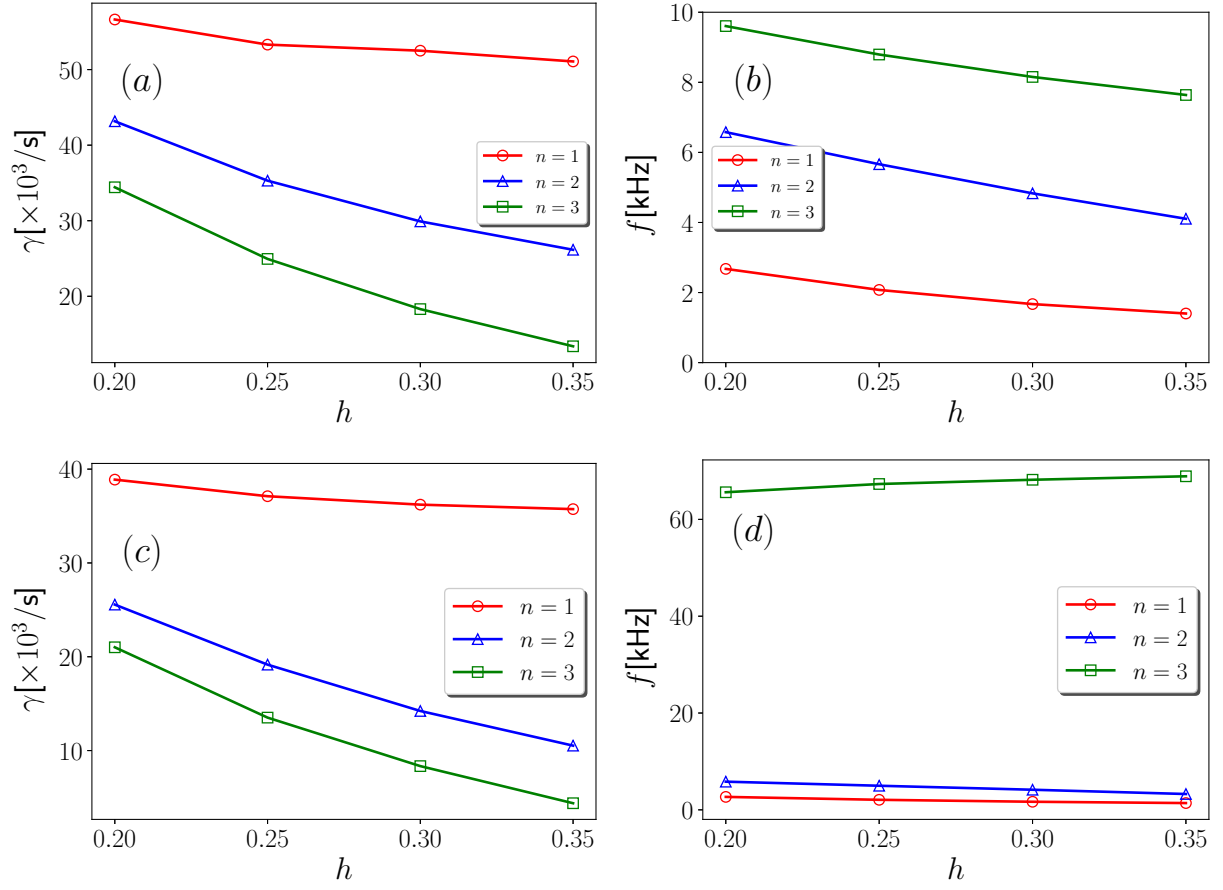


Figure 13: Growth rates [(a) and (c)] and mode frequencies [(b) and (d)] as functions of EP pressure gradient coefficient  $h$  for the 1/1, 2/2 and 3/3 modes, where  $q_0 = 0.9$  and  $\beta_f = 0.1$ . (a) and (b) are based on the M420 equilibrium, (c) and (d) are based on the M452 equilibrium.